**Invited manuscript for a *Frontier* article in *Dalton Transactions***

# Spectroscopic techniques to probe magnetic anisotropy and spin-phonon coupling in metal complexes

Adam T. Hand, Brandon D. Watson-Sanders and Zi-Ling Xue*

*Department of Chemistry, University of Tennessee, Knoxville, Tennessee 37996, USA*

* Corresponding author: xue@utk.edu

## Abstract

Magnetism of molecular quantum materials such as single-molecule magnets (SMMs) has been actively studied for potential applications in the new generation of high-density data storage using SMMs and quantum information science. Magnetic anisotropy and spin-phonon coupling are two key properties of *d*- and *f*-metal complexes. Here, phonons refer to both intermolecular and intramolecular vibrations. Direct determination of magnetic anisotropy and experimental studies of spin-phonon coupling are critical to the understanding of molecular magnetism. This article discusses *our* recent approach in using three complementary techniques, far-IR and Raman magneto-spectroscopies (FIRMS and RaMS, respectively) and inelastic neutron scatterings (INS), to determine magnetic excited states. Spin-phonon couplings are observed in FIRMS and RaMS. DFT phonon calculations give energies and symmetries of phonons as well as calculated INS spectra which help identify magnetic peaks in experimental INS spectra.

## Introduction

Magnetism of metal complexes has been of intense current interest, as it is a key property in many molecular quantum materials such as single-molecule magnets (SMMs).[1-26] In SMMs consisting of metal ions surrounded by ligands, each molecule behaves as a magnet. SMMs are fascinating subjects of study with potential applications in high-density data storage[1-4] and spintronics that investigates the spin of the electron in addition to its negative charge in devices.[27, 28] A wide range of *d* and *f* (mainly lanthanide) metal complexes have been found to possess SMM properties. Research in the SMM areas has been extensively reviewed.[1-26] One basic property of metal complexes with unpaired electrons, critical to SMM performance, is magnetic anisotropy,[24, 25, 29] which reflects the difference in magnetic properties among *x*, *y*, and *z* directions. The characterization of magnetic anisotropy is one focus of this article. Techniques

to characterize magnetic anisotropy in SMMs are recently reviewed by Krzystek and Telser.[30] In this article, two SMMs, $Co^{II}(acac)_2(D_2O)_2$ ($acac^-$ = acetylacetonate, **1**)[31, 32] and $Er^{III}[N(SiMe_3)_2]_3$ (**2**)[33] in Fig. 1, are used here to illustrate magnetic anisotropy and our spectroscopic determination of their anisotropies using a combination of FIRMS, INS, and in the case of **1**, by RaMS.

The local molecular symmetry in **1**, i.e., the symmetry around the $Co^{II}$ ion, is approximately $D_{2h}$, indicating that all three axes *x*, *y* and *z* are different.[31, 32] In **2**, there is a $C_3$ rotation axis through the *z* axis, making the *x* and *y* axes equivalent with 2-fold degeneracy and local $C_{3v}$ symmetry.[33] It should be pointed out that the local molecular symmetry is typically different from the crystallographic symmetry. Crystal structure of $Co(acac)_2(H_2O)_2$, protio isotopologue of **1**, in the monoclinic $P2_1/c$ (No. 14) space group has $C_{2h}$ crystallographic symmetry.[31, 32] Crystal structure of $Er[N(SiMe_3)_2]_3$ (**2**) is disordered over two positions above and below the $N_3$ plane in the molecule, and its trigonal $P\bar{3}1c$ (No. 163) space group has $D_{3d}$ crystallographic symmetry.[33] While the local molecular symmetry may be used to understand magnetic transitions, the crystallographic symmetry is needed to interpret phonon properties and spin-phonon couplings as demonstrated below.

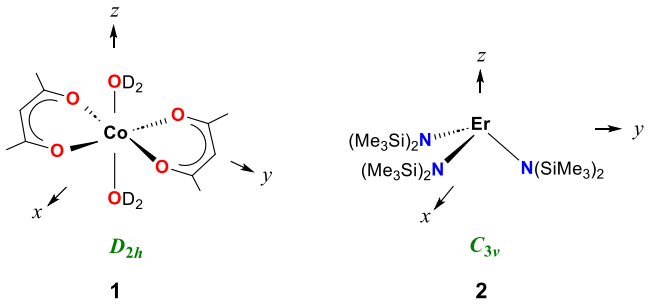


**Fig. 1.** Two complexes with different local molecular symmetries around the metal ions.

As a result of the lowered molecular symmetry (from octahedral $O_h$) in transition metal complex **1**, containing three unpaired electrons ($S$ = 3/2), its spin multiplicity $2S + 1 = 4$ is split into two doublets known as Kramers doublets. The splitting for $Co^{II}(acac)_2(D_2O)_2$ (**1**) into the two doublets $\phi_{1,2}$ and $\phi_{3,4}$, called zero-field splitting (ZFS),[2, 9, 34] is shown in Fig. 2a.[31, 32] In other words, in the absence of an external magnetic field (i.e., zero field), the electronic ground quartet level is split. The anisotropy and Zeeman effect are characterized by the following simplified spin-Hamiltonian:

$$\hat{H}_S = D\left[\hat{S}_z{}^2 - \tfrac{1}{3}S(S+1)\right] + E\left[\hat{S}_x{}^2 - \hat{S}_y{}^2\right] + \mu_B(g_x B_x \hat{S}_x + g_y B_y \hat{S}_y + g_z B_z \hat{S}_z) \qquad (1)$$

where $\hat{S}_i$ = components of the spin operator $\hat{S}$ in the *x*, *y* and *z* directions; *D* and *E* = axial and rhombic ZFS parameters, respectively; $\mu_B$ = electron Bohr magneton; $g_i$ = components of the *g* factor in the *x*, *y* and *z* directions; ***B*** = external magnetic field.

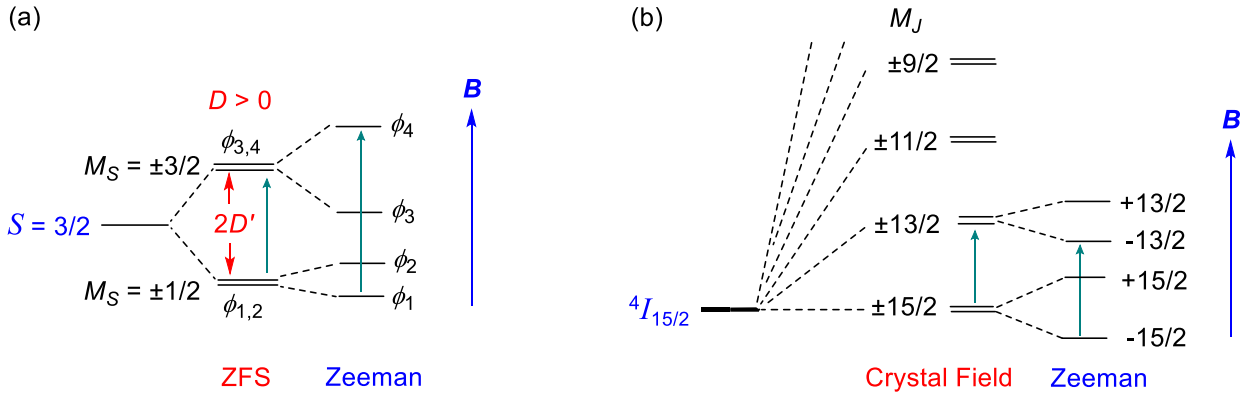


**Fig. 2.** (a) ZFS in **1** into two doublets; $2D' = 2(D^2 + 3E^2)^{1/2}$. The axial ZFS parameter *D* is positive in **1**.[31] The *D* > 0 complexes have the easy-plane (or hard-axis) anisotropy. The ground state $\phi_{1,2}$ are mostly $M_S = \pm 1/2$ which are mixed with $M_S = \pm 3/2$, as a result of $x \neq y$ in **1** (i.e., rhombic ZFS parameter *E*). In other transition metal complexes such as $Co(AsPh_3)_2I_2$[35] not discussed in this article, the $\phi_{1,2}$ and $\phi_{3,4}$ levels are reversed of that in (a), as its *D* < 0. That is, $\phi_{3,4}$ is the ground level, while $\phi_{1,2}$ is the excited level. These *D* < 0 complexes have the so-called easy-axis anisotropy. In both easy-plane and easy-axis anisotropy, the *z* axis is unique (and is the hard- and easy-axis, respectively). (b) Spin-orbit coupled ground state $^4I_{15/2}$ in the lanthanide $Er^{III}$ ion is split by the crystal field of the ligands in $Er[N(SiMe_3)_2]_3$ (**2**) into eight doublets (in the order of increasing energy) $M_J = \pm 15/2, \pm 13/2 \ldots \pm 1/2$.[33] In both (a) and (b), the use of external magnetic field ***B*** leads to the Zeeman splitting.

The significance of ZFS to magnetization and relaxation processes in transition-metal SMMs is that it is an important parameter in barriers for magnetization and relaxation processes, as reviewed in, e.g., refs. 1, 2. For lanthanide-based SMMs, there are also barriers for magnetization and relaxation processes.[3-7, 11, 13-19, 21-25, 36] Recent advancements have contributed to the development of more efficient SMMs with improved stability and control over magnetic behavior.

The anisotropy parameters *D* and *E* are typically determined from fitting variable-

temperature DC (direct current) magnetic susceptibility data from magnetometry. The technique is relatively easy to use and more readily available. However, it is an indirect method using best-fit analysis which may give unreliable results including the sign of *D*, unless multi-field and magnetization data are included.[37] The magnitude of the rhombic parameter *E* is even more difficult to predict without in-depth single-crystal analysis. The fits of DC susceptibility data also often require the inclusion of additional terms such as intermolecular interaction (*zJ*) and temperature independent paramagnetism (TIP) which may complicate the determination of ZFS parameters. Therefore, direct methods to accurately measure ZFS parameters and magnetic excited states are needed. High-field electron paramagnetic resonance (HFEPR) is a powerful tool to measure ZFS up to approximately 33 $cm^{-1}$ for, e.g., the facilities at the US National High Magnetic Field Laboratory (NHMFL).[30, 38-41] Sometimes, simulating HFEPR spectra or combining HFEPR and DC data fitting may measure larger ZFS,[42-46] although using the DC data fitting here may not give reliable ZFS parameters. Using FIRMS,[31, 33, 35, 37, 40, 47-66] frequency-domain-Fourier-transform-terahertz-EPR spectroscopy (FD-FT-THz-EPR),[54, 67, 68] and INS[69-79] to determine magnetic excited levels and anisotropy has been reported. It should be pointed out that magnetic anisotropy of metal complexes has also been determined by cantilever torque magnetometry (CTM)[74, 80-86] which was recently reviewed by Perfetti,[87] angle-resolved magnetometry,[88-91] and μ-SQUID magnetometry used by, e.g., Wernsdorfer and coworkers.[92-95] In addition, electronic structures in metal complexes have been determined by spectroscopic techniques such as magnetic circular dichroism (MCD),[30, 48, 96-99] luminescence,[100-104] and FIRMS. For us, finding spectroscopic methods to directly determine energies of magnetic excited states that are >33 $cm^{-1}$, i.e., large magnetic anisotropy, has been one goal of our recent research.

Another goal of our research is to probe how magnetic and vibrational excited states in SMMs are coupled. Vibrations here include both molecular and lattice vibrations, together known as phonons.[105, 106] Thus, the coupling of the magnetic and vibrational excited states is called spin-phonon coupling. The coupling is a key process in the spin-lattice relaxation of molecules from magnetic excited states. Understanding spin-phonon coupling in SMMs has been of intense current interest,[48, 63, 82, 107-123] including the use of *ab initio* theory of spin-phonon relaxation.[107-112, 115] We have sought to probe spin-phonon coupling by spectroscopies.[31, 33, 35, 53, 54, 124]

This article discusses our recent efforts to use a combination of far-IR and Raman magneto-spectroscopies (FIRMS and RaMS, respectively), and inelastic neutron scattering (INS) to study magnetic anisotropies[31, 33, 35, 40, 53-55, 124-127] and spin-phonon couplings in metal

complexes, determining magnetic excited states and coupling constants, Sometimes, the combined use of FIRMS with high-field EPR (HFEPR) leads to the determination of spin-Hamiltonian parameters *D*, *E* and *g* for transition metal complexes.[37, 54, 55, 57, 59-62] Each of the spectroscopies will be briefly overviewed first, followed by discussion of their use for complexes **1** and **2**. The use of HFEPR has been reviewed[30, 38, 39] and, other than a summary in Table 1, it will not be discussed below.

The facilities we have used include FIRMS[128] and RaMS[129] at NHMFL and INS such as Cold Neutron Chopper Spectrometer (CNCS)[130] and Vibrational Spectrometer (VISION)[131] at Spallation Neutron Source (SNS), Oak Ridge National Laboratory (ORNL), and Disk Chopper Spectrometer (DCS)[132] at NIST Center for Neutron Research (NCNR).

## Overview of spectroscopic techniques to determine magnetic excited states and spin-phonon couplings

Experimental techniques, including FIRMS, RaMS, INS, HFEPR, conventional EPR, and magnetometry, to probe magnetism of *transition metal* complexes are summarized in Table 1 originally published in ref. 35. The overview below also includes FIRMS, RaMS, and INS for both transition metal and lanthanide complexes. Krzystek and Telser recently reviewed techniques to measure large magnetic anisotropy in transition metal complexes relevant to single-molecular magnetism.[30]

### *Far-IR magneto-spectroscopy (FIRMS)*

FIRMS is far-IR spectroscopy, typically in the 12-720 $cm^{-1}$ range, conducted with variable magnetic fields. Far-IR is used, as the magnetic excited levels are often in the energy range. Since there are many IR-active phonons in the range which do not change with the fields, the variable magnetic fields help identify the magnetic peaks which shift with the fields. In a FIRMS experiment, far-IR spectrum is first obtained at 0 T. Then, spectra at different fields are obtained and analyzed to identify the magnetic transitions and spin-phonon couplings. The high-energy side of FIRMS may extend to 720 $cm^{-1}$ into the IR range.

The experimental set up in FIRMS is analogous to that of a typical IR experiment, except that the sample is placed inside a magnet. The light source and the far-IR spectrometer are linked to the sample, often cooled to 5 K. The magnetic transitions are magnetic dipole-allowed and governed by transition moment operators that have the symmetry properties as the rotations ($R_x$, $R_y$, $R_z$) in the character tables of point groups that molecules belong to.[133-135] This is in contrast to an electronic (*d*-*d*) transition, usually giving UV-visible spectra, or a phonon

transition from its ground to the first excited vibrational state (i.e., the so-called a fundamental transition) in IR. Both electronic and phonon transitions are electric dipole-allowed and governed by transition moment operators with the symmetry properties as the Cartesian coordinates (*x*, *y*, *z*) in the character tables.[136]

A powder sample in an eicosane (a waxy chemical) matrix is often used in FIRMS. Sometimes, FIRMS could be obtained from a single crystal, which requires the pre-determination of the crystal orientations. The advantage of using a powder sample is that the operation is relatively easy and fast. However, since the powder contains particles in all directions (*x, y, z*), the interpretation of the spectra may be more challenging. When using powder samples, FIRMS may easily reveal the energies of the excited level such as $2D' = 2(D^2 + 3E^2)^{1/2}$ in Fig. 2a, as shown in the examples below. HFEPR may also be needed to give the *E*/*D* ratio so both *D* and *E* may be obtained.[30, 40, 95]

When Bracket, Richards and coworkers demonstrated over 50 years ago that transitions among ZFS states are magnetic dipole-allowed, they used an earlier version of FIRMS to study ZFS in metalloporphyrin complexes.[133-135] By the time we started using FIRMS to probe SMMs a few years ago,[31] the technique had been used to study magnetic transitions in both transition metal and lanthanide complexes,[47-52] including the works by van Slageren, Dressel, and coworkers.[48-52]

Frequency-domain-Fourier-transform-terahertz-EPR spectroscopy (FD-FT-THz-EPR) is another far-IR setup with external magnetic fields, which differs from FIRMS in the technical outline and specifications.[54, 67, 68] This technique can detect 10–200 $cm^{-1}$ magnetic gaps.

In recent years, FIRMS has been extensively used to probe magnetic excited states in both *d*-[31, 35, 37, 40, 51, 53-62] and *f*-element complexes,[33, 52, 59, 63-66] providing understandings of magnetic anisotropy.

*Raman magneto-spectroscopy (RaMS)*

RaMS is Raman spectroscopy, typically in the 10-8,000 $cm^{-1}$ range, conducted with variable magnetic fields. RaMS facilities[129] are rarer than FIRMS.

Transitions among electronic orbitals have been studied by Raman, and the selection rules for such electronic Raman transitions are known.[137, 138] Since *f*-electrons undergo spin-orbit coupling (SOC), followed by crystal field splitting as shown in Fig. 2b, the transitions among the levels contain both spin/magnetic and orbit/electronic features. Thus, the latter may make transitions among these levels in *f* complexes observable in Raman, since the levels contain some orbital component due to their inherent SOC.[137, 138] For transition metal

complexes, if the angular momentum of *d*-electrons are unquenched, giving first-order SOC (i.e., with no ZFS), transitions among the SOC levels may be similarly observed in Raman. For example, high-spin $d^6$ $[Fe^{II}(H_2O)_6]SiF_6$ containing the nearly perfectly octahedral $Fe(H_2O)_6^{2+}$ ion (with four d electrons in the $t_{2g}$ orbitals) has essentially unquenched orbital angular momentum.[139] Energies of several magnetic energy levels were studied by RaMS by Gnezdilov and coworkers,[140] which were confirmed by other methods.[30, 141, 142] To the best of our knowledge, when we probed RaMS of **1** with ZFS (i.e., quenched angular momentum without first-order SOC), Raman spectroscopy had not been used to probe magnetism in other molecular complexes.

The selection rules for transitions among ZFS, however, are not clear. Very little work has been done in using Raman spectroscopy for such transitions in *d*-complexes. Since ZFS is a result of quenched first-order SOC, transitions among ZFS are expected to be vanishingly small in Raman spectroscopy.

A significant finding in our recent work is that a magnetic transition between ZFS states, although vanishingly weak in Raman spectroscopy, may couple with Raman-active phonons. Thus, the spin-phonon-coupled modes contain both magnetic and phonon features. The phonon features in the coupled modes make the modes observable in Raman. In other words, the magnetic transition is observed in Raman spectroscopy through the coupling with Raman-active phonons.

Raman spectra are typically collected from a single crystal sample, although powders may be used. RaMS has been collected by two instrumental setups at NHMFL.[129] The first is to use a fiber-optic cable to transmit light both to and from the sample with the lower energy cutoff at ~70-100 $cm^{-1}$ for the RaMS facility at NHMFL.[35] In the second, a direct-optics setup uses a collection of calibrated optics on a laser table to guide light both to and from the sample. The latter is complex but a more preferable lower energy limit of ~10 $cm^{-1}$, allowing for the study of low-energy transitions not observable with the fiber-optical setup.[35]

*Inelastic neutron scattering (INS)*

Neutron scatterings for coordination chemistry research, including features of different neutron instruments, have been discussed recently.[143] Dunstan, Mole, and Boskovic have reviewed the use of INS to study lanthanide complexes and SMMs.[69] Earlier use of INS to probe poly-nuclear SMMs was reviewed by McInnes in 2006.[70] Four-dimensional (4-D) INS has been used to probe spin dynamics in molecular magnets.[144, 145]

When an incident neutron beam hits a sample, neutrons are scattered by the sample.

The scattered neutrons may retain the energy as the incident neutron, simply changing the direction, in a process known as elastic neutron scattering. Some of the scattered neutrons may simultaneously transfer energy to the sample when scattering, changing the direction as well as energy of the scattered neutrons, in a process known as inelastic neutron scattering (INS, Fig. 3a).[143]

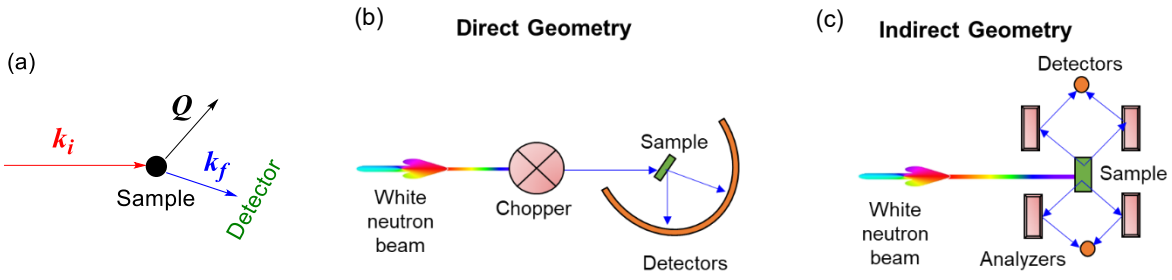


**Fig. 3.** (a) Schematic of the INS process. $\vec{k}_i$ = incident neutron momentum; $\vec{k}_f$ = outgoing (final) neutron momentum; $\vec{Q} = \vec{k}_i - \vec{k}_f$ = vector of momentum transfer; $Q$ = length of $\vec{Q}$. (b) Direct- and (c) Indirect-geometry INS spectrometers. The indirect-geometry spectrometer is shown with scattering angles of 45° and 135°, forward scattering and backscattering, respectively (blue lines). Reproduced with permission from ref. [32]. Copyright 2019, Wiley-VCH.

The use of INS to probe magnetic transitions in a sample is rooted in the fact that when an incident neutron beam hits a sample, the spins of neutrons and unpaired electrons in the sample interact with each other, leading to the excitation of sample from one magnetic energy level to another. The energies of these scattered neutrons are thus lowered. The incident neutron beam may also lead to excitations of the vibrational levels from inelastic scattering with nuclei of atoms in the sample, giving a phonon spectrum. Due to the zero charge, neutrons typically penetrate deeply into a sample.

There are three types of INS instruments:[106] direct-geometry TOF (time-of-flight) spectrometers, indirect-geometry TOF spectrometers, and triple-axis spectrometers (TAS). TOF spectrometers have been widely used in INS relevant to coordination chemistry, especially that of complexes, and powders are the most likely form of the samples.[32, 53] We will focus on direct- and indirect-geometry spectrometers (Fig. 3b-c) which have been used in our research to probe magnetic excitations and phonon properties of both *d*- and *f*-complexes.

In a direct-geometry spectrometer, the incident energy $E_i$ is selected/fixed and $E_f$ is

measured to determine the energy transfer ($\Delta E = E_i - E_f$)[146] as well as its $Q$ range. Cold Neutron Chopper Spectrometer (CNCS)[130] and Disk Chopper Spectrometer (DCS, NIST)[147] are examples of direct-geometry instruments in the USA. Both CNCS and DCS can be used with a magnet. INS, especially the scattering by the direct-geometry spectrometers giving the $Q$ data, is unique in that it can distinguish magnetic peaks from phonons, as they have different $Q$ features.[146, 148, 149] Magnetic peaks decrease in intensity with increased $Q$, while phonons increase in intensity with increased $Q$.[146, 148, 149] Thus, magnetic transitions may be identified by their $Q$ properties. For example, the magnetic transition of Fe(TPP)Cl ($S$ = 5/2, $TPP^{2-}$ = tetraphenylporphyrinate, Fig. 4a) at 12.65(8) $cm^{-1}$ (Fig. 4b) shows that its intensity decreases with increasing $Q$. In contrast, intensities of the peaks >16 $cm^{-1}$ in Fig. 4c increase with increased $Q$, indicating that they are phonons.[127]

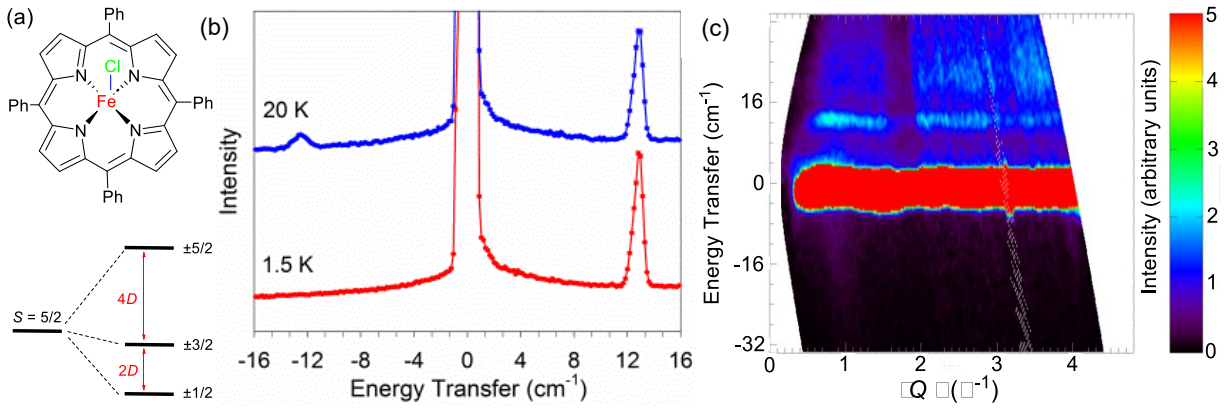


**Fig. 4.** (a) Fe(TPP)Cl and its ZFS splitting ($D$ > 0). (b) INS spectra of Fe(TPP)Cl using a 24.20 $cm^{-1}$ incident neutron beam[127] at CNCS.[130] The small peak at −12.65(8) $cm^{-1}$ in the 20 K spectrum is from neutrons at the excited ±3/2 level relaxing back to the ground ±1/2 level, giving the energy to the incident neutrons. (c) Change in the peak intensities vs $Q$ at 1.5 K. Incident neutron energy: 80.66 $cm^{-1}$. Reproduced with permission from ref. 127. Copyright 2014, American Chemical Society.

In an indirect-geometry INS spectrometer (Fig. 3c) at SNS, ORNL, a “white” beam (i.e., neutrons with a wide energy range) is used. Thus, the neutron flux is much larger than that in the direct-geometry INS spectrometer, making the data collection much shorter. $E_i$ is determined by the time the neutron reaches the detector through the time of flight (TOF).[106] VISION is an example that gives a broad energy transfer range of ~4 to 4000 $cm^{-1}$ with high energy/spectral resolution.[150-152]

INS was used to probe di- and poly-nuclear complexes, including SMMs which usually have a large spin *S* but a small ZFS parameter *D*.[153-162] The magnetic separations in these complexes tend to be small.[70, 153, 161, 162] For example, INS spectrum of $[Fe_8O_2(OH)_{12}(tacn)_6]Br_8$ (named $Fe_8$; *S* = 10; tacn = 1,4,7-triazacyclononane) shows that the magnetic transition is about 3.75 $cm^{-1}$.[153] INS has been used, including together with toque manetometry,[79] to study magnetic excitations. For SMMs with one magnetic ion, called single-ion magnets (SIMs) with typically much larger anisotropy, INS has been used to probe their magnetic properties, including the determination of magnetic excited states.[71-79] For example, for **1**, $D > 50$ $cm^{-1}$, indicating it has much larger ZFS than those in many poly-nuclear complexes. The challenge for us when we started using INS to characterize SIMs in the mid-2010s was how to identify magnetic peaks of such high energies in INS spectra.

It should be pointed out that, while INS is a useful tool for magnetic studies, it typically needs more samples (0.5-2 g) than FIRMS and RaMS. Sometimes, deuterated samples are required due to the large background in INS spectra from hydrogen atoms.[163, 164] In addition, neutron instruments are only available at national laboratories such as ORNL and NCNR.

*Spin-phonon coupling*

Phonons in far-IR and Raman spectroscopies at 0 T follow different selection rules, giving IR-active and Raman-active phonon spectra, respectively. As indicated earlier, crystal structure of protio $Co(acac)_2(H_2O)_2$ belongs to the monoclinic $P2_1/c$ (No. 14) space group with $C_{2h}$ crystallographic symmetry.[31, 32] In addition, molecules of $Co(acac)_2(H_2O)_2$ are at the center of inversion *i* in the $C_{2h}$ group.[31] Thus, IR-active and Raman-active phonons in their spectra have *u*- and *g*-symmetry, respectively. In contrast, inelastic neutron scattering (INS) does not have such a symmetry-based selection rule, as it is based on kinetic energy transfer from incident neutrons to molecules in the sample. Thus, all phonons are active in INS. In addition, quantitative (frequencies and intensities) computation of the neutron vibrational spectrum by periodic DFT calculations using VASP (Vienna Ab initio Simulation Package) is feasible.[31] The calculated INS phonon spectrum can be directly and quantitatively compared to the experimental INS spectra.[31, 35, 53, 54] The latter show both magnetic and phonon peaks. Thus, a comparison between the calculated phonon spectrum and the experimental spectrum helps identify the magnetic peak, as this peak is not in the calculated phonon spectrum.

Spin-phonon coupling is observed in FIRMS and RaMS in the form of an avoided crossing. A schematic view of the spin–phonon coupling is given in Fig. 3 of ref. 31, while Fig. 5a here shows a simpler representation. In essence, spin–phonon coupling occurs when the

magnetic excited state $\varphi_{magnetic}$ and phonon excited state $\varphi_{phonon}$ have the same symmetry. When these states are close in energy, they interact to form two new, spin-phonon coupled states, one ($\Psi_+$) with higher energy and one ($\Psi_-$) with lower energy than the energies of $\varphi_{magnetic}$ and $\varphi_{phonon}$ states. The two new states $\Psi_+$ and $\Psi_-$ carry both magnetic and phonon features. Such coupling is similar to how two atomic orbitals (AOs), or combinations of AOs, interact to form molecular orbitals (MOs) – The energy of the bonding MO is lower than the AOs, and the antibonding MO is higher than the AOs.

Zeeman effect leads to the energy shift of the magnetic excited state $\varphi_{magnetic}$ and thus the coupling with the phonon excited state. Fig. 5b illustrates how the spin-phonon coupling of a magnetic state, which shifts to higher energy (known as the blue shift), changes with the magnetic field. The coupling is the strongest when the energies of the two states are the closest. The magnetic excited state gradually gains the phonon features, while the phonon excited state receives more magnetic properties. At higher magnetic fields, the magnetic excited state eventually becomes phonon, while the phonon excited state becomes magnetic. During the coupling and change with the magnetic fields, the two states never cross each other, and this process is thus called an avoided crossing.

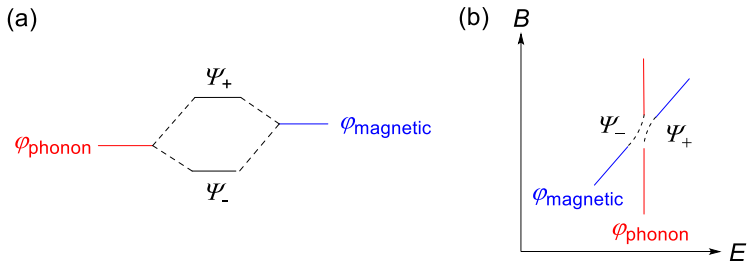


**Fig. 5.** (a) Schematic view of the spin–phonon coupling. $\varphi_{magnetic}$ and $\varphi_{phonon}$ represent eigenfunctions of the magnetic state and phonon, respectively. $\Psi_+$ and $\Psi_-$ are eigenfunctions of the two spin-phonon coupled states. (b) Energy change ($E$) of the spin-phonon coupling with the external magnetic field $B$ ($B$ = magnitude of $\boldsymbol{B}$).

Spin-phonon coupling can be fit using Eq. 2:

$$\hat{H} = \begin{pmatrix} E_{sp} & \Lambda \\ \Lambda & E_{ph} \end{pmatrix} \quad (2)$$

where $E_{sp}$ and $E_{ph}$ = expected energies of the spin/magnetic and phonon excitations, respectively; $\Lambda$ = spin-phonon coupling constant.

The matrix is solved to give two eigenvalues $E_{\pm}$ in the secular Eq. 3.

$$\begin{vmatrix} E_{sp} - E_{\pm} & \Lambda \\ \Lambda & E_{ph} - E_{\pm} \end{vmatrix} = 0 \quad (3)$$

Solutions $E_+$ and $E_-$ from Eq. 3 are the energies of the two states during the avoided crossing, yielding two peaks repelling each other. A model based on the vibronic coupling is given in ref. 31, providing more characterization of spin-phonon coupling.

**Characterization of SMMs 1-2 – Two examples**

The two complexes demonstrate how we have probed magnetic anisotropy and spin-phonon coupling from different perspectives. $Co(acac)_2(D_2O)_2$ (**1**) is an $S = 3/2$ transition metal complex with ZFS (Fig. 2a).[31, 32, 165] $Er[N(SiMe_3)_2]_3$ (**2**) is a lanthanide complex with multiple crystal-field states from the spin-orbit coupled ground state $^4I_{15/2}$ shown in Fig. 2b.[33, 166]

*$Co(acac)_2(D_2O)_2$ (**1**)*

$Co(acac)_2(D_2O)_2$ (**1**) illustrates how FIRMS,[31] RaMS,[31] and INS[32] were used to characterize magnetic excited states and spin-phonon coupling in the complex. Deuterated water ligands in **1** make its phonon properties different from its isotopologues $Co(acac)_2(H_2O)_2$ and $Co(acac\text{-}d_7)_2(D_2O)_2$.[31] To our knowledge, the results of **1** and its isotopologues are the first direct observation of spin-phonon couplings in Raman spectra of a molecular compound and their quantification.[31]

FIRMS and RaMS spectra of **1** and their contour maps are given Fig. 6. The $Co^{II}$ ion in the molecule of **1** is at the inversion center *i* (of the crystallographic $C_{2h}$ point group). The $Co^{II}$ d orbitals have *g* symmetries. Since the ZFS states $\phi_{1,2}$ and $\phi_{3,4}$ in Fig. 2a are from 3*d* orbitals in the $Co^{II}$ ion, the states have the *g* symmetry. Since rotations (or magnetic dipoles) ($R_x$, $R_y$, $R_z$) have *g* symmetries, the magnetic-dipole-allowed ZFS transition from $\phi_1$ to $\phi_4$ (Fig. 2a), a $g \rightarrow g$ transition, is expected to be observable in FIRMS. Although the transition is not strong in far-IR spectra in Fig. 2a as it overlaps with a strong IR-active phonon, the contour plot in Fig. 6b, highlighting differences among the far-IR spectra at different magnetic fields, clearly shows that the ZFS transition as Trace 1 starts at ($2D'$ =) 114 $cm^{-1}$ at 0 T. The transition from $\phi_1$ to $\phi_4$ in Fig. 2a is magnetic-dipole-allowed due to the mixing of the ZFS states from the rhombic ZFS parameter *E*. Another magnetic transition, Trace 2, is shown in Fig. 6b. From analyses by a

vibronic coupling model detailed in ref. 31, Trace 2 is the transition from $\phi_1$ to $\phi_3$. The $E/D$ = 0.31 from EPR was reported earlier for Co(acac-$d_7$)$_2$($H_2O$)$_2$.[165]

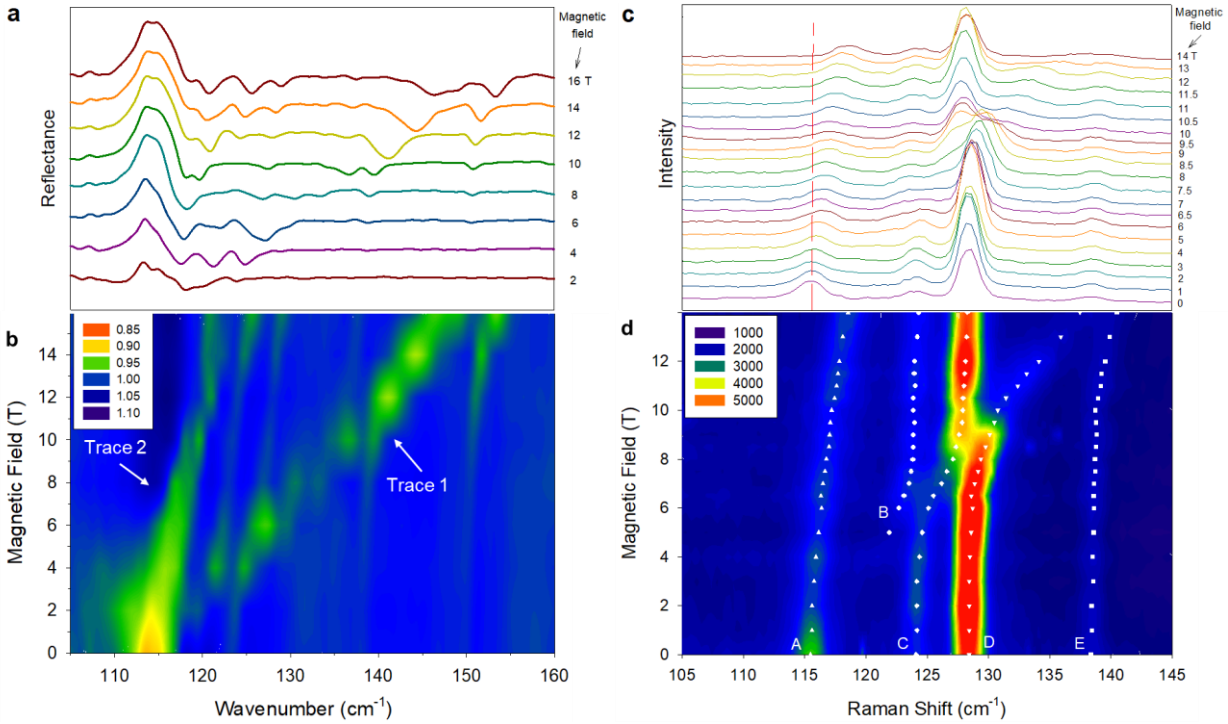


**Fig. 6.** FIRMS and RaMS spectra and contour maps of **1**. (a) Normalized far-IR reflectance spectra at different magnetic fields. (b) Contour plot of the far-IR spectra. (c) Raman spectra at different magnetic fields. The vertical line indicates Peak **A**, a phonon, marked in Fig. 6b. (d) Contour map from the Raman spectra. Peak **B** is the magnetic transition. Peaks **C**, **D**, and **E** are phonons. Reproduced from ref. 31.

For **1** in crystallographic $C_{2h}$ point group, phonons have either $g$ ($A_g$/$B_g$) or $u$ ($A_u$/$B_u$) symmetries. The former are Raman-active and latter IR-active. Since the magnetic transition from $\phi_1$ to $\phi_4$ (Trace 1) is a $g \rightarrow g$ transition, it is coupled with Raman-active $g$ phonons in spin-phonon couplings. Trace 1 is shown as Peak **B** in Fig. 6d. At 0 T, it is coupled to phonon Peak **A**, pushing **A** to the left, although **B** itself at 0 T is too weak to be observed. With increasing magnetic fields, **B** blue-shifts gradually to higher energies. As **B** moves away, **A** shifts to the right at 14 T, back to its position when there is no coupling with **B**.

At about 6 T in Fig. 6c-d, **B** is close to phonon Peak **C**, undergoing another spin-phonon coupling now with **C**. The coupling makes the magnetic transition contain partial $g$-phonon features. Thus, both coupled peaks are observed in the Raman spectra. **B** gradually becomes a

phonon over 8 T, while **C** turns to a magnetic peak moving to the right. **C**, now magnetic, then couples with the strong phonon **D**, leading to the observation of two coupled peaks at 8-10 T. At this stage, the original phonon intensity of **D** is shared between the two coupled peaks. Afterwards, **C** gradually becomes a phonon, while **D** turns into a magnetic peak shifting to higher energy. Our study showed for the first time distinct couplings of *g* phonons in $Co(acac)_2(D_2O)_2$ (and its isotopologues) with excited ZFS levels. Using Eqs. 2–3. The spin-phonon couplings in RaMS could be fit as shown as the dotted lines in 7d, generating the coupling constants $|\Lambda|$ = ~1-2 $cm^{-1}$.[31] The absolute values indicate that we do not know whether the coupling constants are positive or negative.

Atanasov and Neese have developed a vibronic coupling model, supported by *ab initio* electronic structure calculations, to rationalize the behavior of the coupled Raman peaks and quantify the spin-phonon couplings.[31] The results from the model are consistent with those from the RaMS experiments.

INS studies were conducted on partially deuterated **1** using VISION and per-deuterated $Co(acac\text{-}d_7)_2(D_2O)_2$ using both VISION and DCS (Disk Chopper Spectrometer) at NCNR.[32] Spectra of $Co(acac\text{-}d_7)_2(D_2O)_2$ are given in Fig. 7. H atoms give large incoherent scattering, contributing to background, and make it more challenging to identify magnetic peaks. It should be noted that magnetic peaks have been identified in protio samples, as shown in INS spectra of Fe(TPP)Cl in Fig. 4.[127]

Variable-temperature (VT) INS spectra of **1** at VISION were processed by Bose-corrections to identify magnetic peak from those of phonons. Electrons (giving a magnetic peak) and phonons are fermions and bosons, respectively. Thus, they show different temperature dependences. Bose-correction makes phonon peaks at different temperatures have similar profile and baseline intensity. In Fig. 7a, the peak at 114 $cm^{-1}$ clearly stands out and was identified to be magnetic. Variable-field INS spectra of **1** at DCS in Fig. 7b shows that the peak at 114 $cm^{-1}$ is shifted away, when 10 T magnetic field is applied. This feature shows the peak to be magnetic.

We have performed DFT phonon calculations that give calculated INS phonon spectrum as well as energies of phonons and their *g*/*u* symmetries.[31] Comparisons of the calculated INS phonon spectrum with the experimental INS spectra help reveal the magnetic peaks in the experimental INS spectra,[31, 33, 35, 54] as the peaks are not in the calculated phonon spectrum (which gives phonons only). The phonon calculations also lead to movies of the phonons to visualize the vibrations.[31, 35, 53, 54]

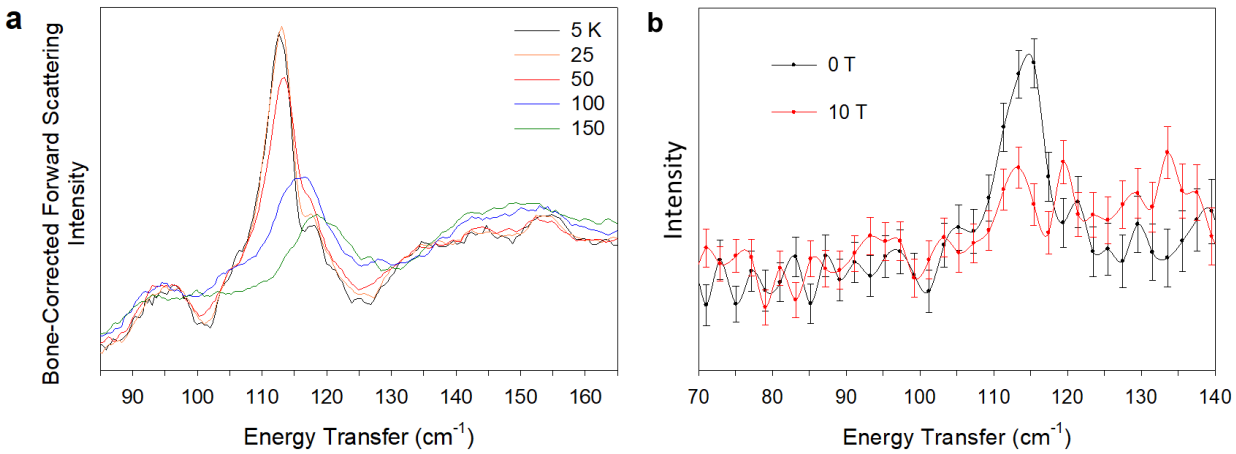


**Fig. 7.** INS spectra of Co(acac-$d_7$)$_2$($D_2O$)$_2$. (a) VT INS spectra at VISION. (b) INS spectra by DCS at 0 and 10 T. Reproduced with permission from ref. 32. Copyright 2019, Wiley-VCH.

*Er[N(SiMe$_3$)$_2$]$_3$ (**2**)*[33]

For the lanthanide complex **2**, with $M_J$ = ±15/2 doublet as the ground state as shown in Fig. 2b,[166] FIRMS spectra in Fig. 8a at different magnetic fields reveal at least three magnetic excitations at 0 T at 104 cm$^{-1}$, ~180 cm$^{-1}$, and 245 cm$^{-1}$ from the transitions from the ground state to the first three excited states, $M_J$ = ±13/2, ±11/2, and ±9/2, respectively.[33] The transition between the ground and first excited states at 104 cm$^{-1}$ is also observed in variable-field INS in Fig. 8b, moving to higher energy with increasing magnetic field. Er[N(SiMe$_3$)$_2$]$_3$ (**2**) is very air-sensitive, making its characterization by Raman spectroscopy challenging. RaMS was used to study **2**, but it did not reveal the magnetic peaks.[33] The air-sensitivity or fluorescence of the sample in the RaMS study may have played a role.

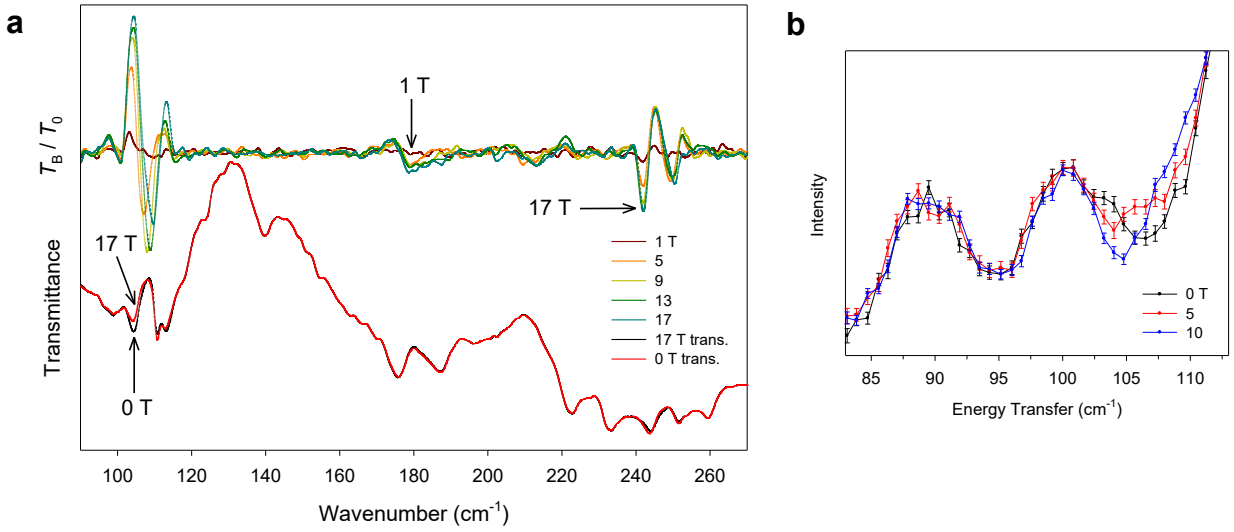


**Fig. 8.** (a) Bottom: Far-IR transmission spectra of a crystal sample of **2** at 0 T (black) and 17 T (red). Top: The far-IR spectra at 1, 5, 9, 13, and 17 T normalized to the zero-field spectrum. (b) INS spectra by DCS at 1.7 K at 0 (black), 5 (red), and 10 T (blue), showing the magnetic peak at 104 $cm^{-1}$. Reproduced with permission from ref. 33. Copyright 2020, American Chemical Society.

Spin-phonon couplings involving the magnetic transitions at 104 $cm^{-1}$ and 245 $cm^{-1}$ with IR-active phonons were observed in FIRMS spectra in Fig. 9.[33] Using Eqs. 2-3 to fit the couplings yields the coupling constants $|\Lambda|$ = 3 $cm^{-1}$.

DFT phonon calculations give phonon symmetries and calculated INS spectrum to compare with the INS spectra from VISION (not shown here).[33]

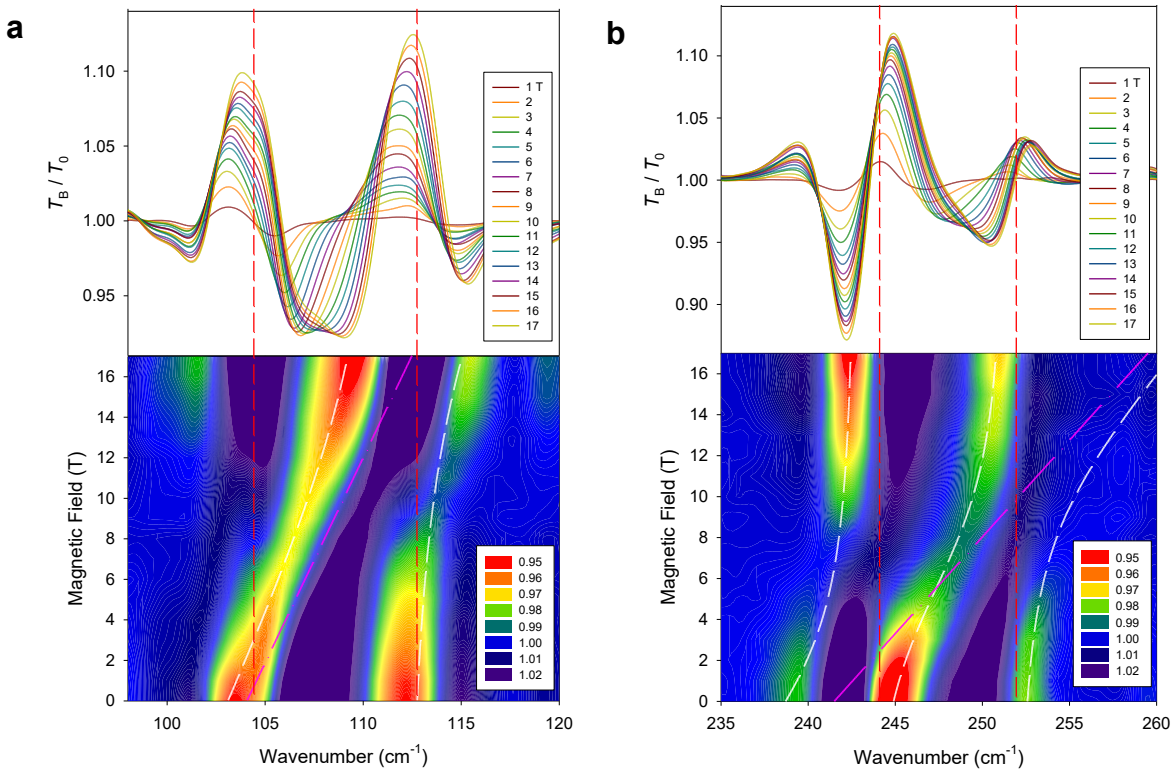


**Fig. 9**. Far-IR spectra near magnetic excitations in a powder sample of **2**. (a) Spectra near 104 cm$^{-1}$. (b) Spectra near 245 cm$^{-1}$. Top: Transmission ($T_B$) normalized to the zero-field spectrum ($T_0$); Bottom: Contour plot of the normalized transmission (by average). White lines represent results of the spin-phonon coupling fitting. Pink lines represent the shift of the uncoupled magnetic peak used for the coupling parameters $E_{sp}$. Vertical red lines indicate approximate zero field positions of dominant phonon excitations. Reproduced with permission from ref. 33. Copyright 2020, American Chemical Society.

## Conclusions

Energies of magnetic transitions in many SMMs are in the range that can be characterized by FIRMS, RaMS, and INS. These spectroscopic techniques provide a picture of magnetic energy levels in metal complexes and spin-couplings. Such studies are critical to comprehend magnetic properties of the SMMs, including their magnetic relaxations. This approach, with various complementary spectroscopies, could be utilized in the studies of similar *d*- and *f*- complexes by probing the magnetic transitions and revealing spin−phonon couplings. The experimental results, together with electronic structure calculations, phonon calculation, and models of spin-phonon coupling, provide comprehensive understandings of the magnetic properties of metal complexes and help design better SMMs.

Looking into the future, more use of oriented single crystals of SMMs in FIRMS[63] and INS experiments is expected to give a better characterization of magnetic and phonon properties, including magnetic anisotropy, and spin-phonon coupling. Such experiments are more challenging and typically take longer times to conduct. In addition, orientations of the single crystals need to be determined by single-crystal X-ray or neutron diffraction. For RaMS, theoretical studies are needed to understand the role of Raman spectroscopy plays in magnetic transitions of SMMs. In addition, how crystal and molecular symmetries affect spin-phonon couplings in SMMs requires more experimental and theoretical studies. Given that *ab initio* methods to predict spin-phonon relaxation have been actively studied, combing the experimental/spectroscopic results of spin-phonon coupling studies with the calculated results by the *ab initio* methods[63] is expected to give a better understanding of the relaxation mechanisms.

**Conflicts of Interest**

There are no conflicts to declare.

**Acknowledgments**

The authors thank the past and current students in the research group and collaborators for their contributions and the US National Science Foundation (CHE-2055499) for financial support. We appreciate the opportunities to use the facilities at National High Magnetic Field Laboratory (NHMFL), Oak Ridge National Laboratory (ORNL), and NIST Center for Neutron Research (NCNR).

**Table 1.** Experimental techniques to probe magnetism of transition metal complexes.[a,b] Reproduced with permission from ref. 35. Copyright 2022, American Chemical Society.

| Technique | Parameter(s) of Interest | Approx. Energy Range ($cm^{-1}$) | Features |
|---|---|---|---|
| Far-IR magneto-spectroscopy (FIRMS)[31, 48, 167] | • $D'$ for Kramers ions<br>• $D$, $E$ for non-Kramer ions | Typically 12-720 $cm^{-1}$ [c] | • Revealing magnetic transitions, i.e., energies of magnetic excited levels for complexes with either unquenched or quenched orbital angular momenta.<br>• For complexes with zero-field splitting (ZFS) (i.e., quenched orbital angular momenta), direct and precise determination of $D'$ or $D$, $E$<br>• Broad spectral range.<br>• Revealing spin-phonon couplings with IR-active phonons[d] (such as *u* phonons in centrosymmetric crystals).<br>• Appearance of phonons near the magnetic peak potentially complicating direct observation of the latter due to spin-phonon coupling.<br>• Small amount of powder samples (≤5 mg) or single crystals; Samples typically disposed after use.<br>• Resolution at 0.3 $cm^{-1}$ for the facilities at NHMFL.[b,168]<br>• Single temperature of ~5.5 K for the facilities at NHMFL.[168] |
| Raman magneto-spectroscopy (RaMS)[31] | $\|D'\|$<br>$g_x$, $g_y$, $g_z$ | 10-3000 $cm^{-1}$ (direct optic probe)<br><br>70-3000 $cm^{-1}$ (fiber optic probe) based on the facilities at NHMFL[169] | • Relatively broad energy range.<br>• Revealing spin-phonon couplings with Raman-active phonons (such as *g*- phonons in centrosymmetric crystals).<br>• A small crystal required, although powder samples may be used.<br>• Appearance of phonons near the magnetic peak potentially complicating direct observation of the latter.<br>• Selection rules for ZFS transitions in Raman spectroscopy not well understood.<br>• Limited instrumental availability, requiring Raman filters and optical systems to observe low energy peaks.<br>• Resolution at 1-2 $cm^{-1}$ for the facilities at NHMFL.[169] |
| Inelastic neutron scattering (INS)[143, 170] | $\|D'\|$ | 10-8000 $cm^{-1}$ | • Revealing magnetic transitions, i.e., energies of magnetic excited levels for complexes with either unquenched or quenched orbital angular momenta.<br>• For complexes with ZFS, direct determination of $\|D'\|$; Sign of $D$ when $M_S$ = 5/2 and 2[127] by an direct-geometry INS spectroscometer[143] such as CNCS[171] at ORNL[b] or DCS[172] at NCNR.[b]<br>• Broad energy range for indirect-geometry spectrometers[143] such as VISION[173] at ORNL.<br>• Distinguishing between magnetic and phonon transitions via temperature-,[54] field-,[53] and/or $\|\boldsymbol{Q}\|$[e]-dependences,[127] depending on whether the spectrometer is direct- or indirect-geometry.<br>• Truly zero-field techniques requiring no magnet, although a magnet may be used to reveal additional properties; The magnet often blocks large portions of neutron detectors, leading to longer data acquisition and increased background. |

| | | | |
|---|---|---|---|
| | | | • No symmetry-based selection rule for phonons, leading to the observation of all phonon peaks.<br>• Resolutions varied depending on the energy ranges.[171, 173]<br>• DFT-calculated phonon INS spectra by, e.g., VASP program for comparison with experimental INS spectra, helping identify magnetic peaks.[54]<br>• Limited instrumental availability.<br>• Large amount of powder samples (typically ≥0.5 g).<br>• Samples *possibly* becoming radioactive, requiring decay times before reuse. |
| High-field, high-frequency EPR (HFEPR)[38] | $D$, $E$, $g_x$, $g_y$, $g_z$ | Typically <33 $cm^{-1}$ | • Highly accurate, direct determination of $D$ and $E$ parameters and $g$ tensors.<br>• Only magnetic-dipole-allowed transitions observed; However, phonons may give complex spectra through spin-phonon couplings.<br>• When $D < 0$, $E = 0$ (with no mixing of states, e.g., shown in Figure 1), the transition within the ground doublet ($-M_S \rightarrow +M_S$) is forbidden.[f,174]<br>• Compatible with Kramers and non-Kramers complexes depending on accessible frequencies and fields.<br>• Limited energy range: ZFS transitions up to 30 $cm^{-1}$ in non-Kramers ($S$ = integers) and 15 $cm^{-1}$ in Kramers complexes for the user facilities at NHFML<br>• Limited instrumental availability.<br>• ZFS indirectly determined by multi-parameter fits to the field/frequency dependencies of the resonances.<br>• Small amount of powder samples (≤100 mg) or single crystals.<br>• Powder samples may be reused. |
| Conventional EPR (X- and Q-band)[175, 176] | $D$, $E$, $g_x$, $g_y$, $g_z$ | <0.3 $cm^{-1}$ (X-band) or 1.2 $cm^{-1}$ (Q-band) | • Widely available instrumentation compared to HFEPR.<br>• Limited energy range.<br>• Typically incompatible with non-Kramers or easy-axis Kramers ions (i.e., $D < 0$, $E = 0$) due to frequency and field limitations (such systems are called *EPR-silent*).<br>• Small amount of powder samples (≤100 mg) or single crystals.<br>• Powder samples or single crystals which may be reused. |
| Magnetometry (Magnetic susceptibility measurement)[30, 177] | **DC:**[g]<br>$D$, $E$, $g$, $C$, $\theta$, $\mu_{eff}$, $M_s$, $M_r$, $H_c$, $T_C$, $T_N$<br><br>**AC:**[h]<br>$\tau$, Relaxation mechanisms including the direct, Raman, and Orbach processes, $U_{eff}$ | | • Suitable for a variety of compounds with no limits of ZFS<br>• Bulk, non-resonant technique likely prone to error; Impurities may also contribute to the data, while spectroscopies may detect the impurities and samples individually<br>• Indirect determination of ZFS parameters<br>• Challenging to measure accurately compounds with small magnetic moments<br>• Difficult to distinguish the sign of $D$<br>• Small amount of powder samples (≤100 mg) or single crystals<br>• Sensitive to precise determination of sample mass and background correction from the sample holder<br>• Samples reusable for other studies<br>• Widely available instrumentation |

[a] $D$ and $E$ = Axial and rhombic anisotropic parameters, respectively; $|D'| = (D^2 + 3E^2)^{1/2}$; $g$ = Lande factor (or $g$-factor); $g_x$, $g_y$, $g_z$ (also labled $g_{xx}$, $g_{yy}$, $g_{zz}$) = Components in the $\boldsymbol{g}$ tensor.

[b] NHMFL = National High Magnetic Field Laboratory; ORNL = Oak Ridge National Laboratory; NCNR = NIST Center for Neutron Research.

[c] The instrument is also available in the IR range up to 6000 $cm^{-1}$.

[d] Phonons include vibrations of both molecules and crystal lattice.

[e] $\boldsymbol{Q}$ = Vector of momentum transfer in neutron scattering processes.[143]

[f] $\Delta M_S$ = 2, 3, 4, and 5 for transitions within the ground doublet in $S$ = 1, 3/2, 2, and 5/2 complexes, respectively, while the selection rules for magnetic-dipole-allowed transitions are $\Delta M_S = 0, \pm 1$.[174] In fact, when $E$ is small, leading to little mixing of the states, e.g., shown in Figure 1, it may still be difficult to observe the transitions within the ground doublet.

[g] $C$ = Curie constant, $\theta$ = Weiss constant, $\mu_{eff}$ = Effective moment, $M_s'$ = Saturation magnetization, $M_r$ = Remnant magnetization, $H_c$ = Coercive field, $T_C$ = Curie temperature, $T_N$ = Neel temperature.

[h] $\tau$ = Relaxation time, $U_{eff}$ = Effective energy barrier for spin reversal in the Orbach processes.

**References**


1. J. M. Frost, K. L. M. Harriman and M. Murugesu, *Chem. Sci.*, 2016, **7**, 2470.
2. F. Neese and D. A. Pantazis, *Faraday Discuss.*, 2011, **148**, 229-238.
3. S. Gao, *Molecular Nanomagnets and Related Phenomena*, Springer, 2015.
4. M. Feng and M.-L. Tong, *Chem. Eur. J.*, 2018, **24**, 7574.
5. N. F. Chilton, *Annu. Rev. Mater. Res.*, 2022, **52**, 79-101.
6. E. Coronado, *Nat. Rev. Mater.*, 2020, **5**, 87-104.
7. A. Zabala-Lekuona, J. M. Seco and E. Colacio, *Coord. Chem. Rev.*, 2021, **441**, 213984.
8. J. Juráková and I. Šalitroš, *Monatsh. Chem.*, 2022, **153**, 1001-1036.
9. R. Boča, C. Rajnák and J. Titiš, *Magnetochemistry*, 2023, **9**, 100.
10. A. Sarkar, S. Dey and G. Rajaraman, *Chem. Eur. J.*, 2020, **26**, 14036-14058.
11. M. Georgiev and H. Chamati, *ACS Omega*, 2022, **7**, 42664-42673.
12. P. Kumar Sahu, R. Kharel, S. Shome, S. Goswami and S. Konar, *Coord. Chem. Rev.*, 2023, **475**, 214871.
13. J.-P. Sutter, V. Béreau, V. Jubault, K. Bretosh, C. Pichon and C. Duhayon, *Chem. Soc. Rev.*, 2022, **51**, 3280-3313.
14. J. D. Rinehart and J. R. Long, *Chem. Sci.*, 2011, **2**, 2078-2085.
15. D. N. Woodruff, R. E. P. Winpenny and R. A. Layfield, *Chem. Rev.*, 2013, **113**, 5110-5148.
16. S. T. Liddle and J. van Slageren, *Chem. Soc. Rev.*, 2015, **44**, 6655-6669.
17. P. Zhang, L. Zhang and J. Tang, *Dalton Trans.*, 2015, **44**, 3923-3929.
18. J. Lu, M. Guo and J. Tang, *Chem. Asian J.*, 2017, **12**, 2772-2779.
19. J.-L. Liu, Y.-C. Chen and M.-L. Tong, *Chem. Soc. Rev.*, 2018, **47**, 2431-2453.
20. G. A. Craig and M. Murrie, *Chem. Soc. Rev.*, 2015, **44**, 2135-2147.
21. H. L. C. Feltham and S. Brooker, *Coord. Chem. Rev.*, 2014, **276**, 1-33.
22. R. A. Layfield, *Organometallics*, 2014, **33**, 1084-1099.
23. S. G. McAdams, A.-M. Ariciu, A. K. Kostopoulos, J. P. S. Walsh and F. Tuna, *Coord. Chem. Rev.*, 2017, **346**, 216-239.
24. N. F. Chilton, *Inorg. Chem.*, 2015, **54**, 2097-2099.
25. L. Ungur and L. F. Chibotaru, *Inorg. Chem.*, 2016, **55**, 10043-10056.
26. A. Raza and M. Perfetti, *Coord. Chem. Rev.*, 2023, **490**, 215213.
27. L. Bogani and W. Wernsdorfer, *Nat. Mater.*, 2008, **7**, 179-186.
28. S. Sanvito, *Chem. Soc. Rev.*, 2011, **40**, 3336-3355.
29. L. Ungur and L. F. Chibotaru, *Phys. Chem. Chem. Phys.*, 2011, **13**, 20086-20090.

30. J. Krzystek and J. Telser, *Dalton Trans.*, 2016, **45**, 16751-16763.
31. D. H. Moseley, S. E. Stavretis, K. Thirunavukkuarasu, M. Ozerov, Y. Cheng, L. L. Daemen, J. Ludwig, Z. Lu, D. Smirnov, C. M. Brown, A. Pandey, A. J. Ramirez-Cuesta, A. C. Lamb, M. Atanasov, E. Bill, F. Neese and Z.-L. Xue, *Nat. Commun.*, 2018, **9**, 2572.
32. S. E. Stavretis, Y. Cheng, L. L. Daemen, C. M. Brown, D. H. Moseley, E. Bill, M. Atanasov, A. J. Ramirez-Cuesta, F. Neese and Z.-L. Xue, *Eur. J. Inorg. Chem.*, 2019, **2019**, 1119-1127.
33. D. H. Moseley, S. E. Stavretis, Z. Zhu, M. Guo, C. M. Brown, M. Ozerov, Y. Cheng, L. L. Daemen, R. Richardson, G. Knight, K. Thirunavukkuarasu, A. J. Ramirez-Cuesta, J. Tang and Z.-L. Xue, *Inorg. Chem.*, 2020, **59**, 5218-5230.
34. R. Boča, *Coord. Chem. Rev.*, 2004, **248**, 757-815.
35. D. H. Moseley, Z. Liu, A. N. Bone, S. E. Stavretis, S. K. Singh, M. Atanasov, Z. Lu, M. Ozerov, K. Thirunavukkuarasu, Y. Cheng, L. L. Daemen, D. Lubert-Perquel, D. Smirnov, F. Neese, A. J. Ramirez-Cuesta, S. Hill, K. R. Dunbar and Z.-L. Xue, *Inorg. Chem.*, 2022, **61**, 17123-17136.
36. A. Chiesa, F. Cugini, R. Hussain, E. Macaluso, G. Allodi, E. Garlatti, M. Giansiracusa, C. A. P. Goodwin, F. Ortu, D. Reta, J. M. Skelton, T. Guidi, P. Santini, M. Solzi, R. De Renzi, D. P. Mills, N. F. Chilton and S. Carretta, *Phys. Rev. B*, 2020, **101**, 174402.
37. L. Devkota, D. J. SantaLucia, A. M. Wheaton, A. J. Pienkos, S. V. Lindeman, J. Krzystek, M. Ozerov, J. F. Berry, J. Telser and A. T. Fiedler, *Inorg. Chem.*, 2023, **62**, 5984-6002.
38. J. Krzystek, A. Ozarowski and J. Telser, *Coord. Chem. Rev.*, 2006, **250**, 2308-2324.
39. G. R. Eaton and S. S. Eaton, *Appl. Magn. Reson.*, 1999, **16**, 161-166.
40. A. N. Bone, S. E. Stavretis, J. Krzystek, Z. Liu, Q. Chen, Z. Gai, X. Wang, C. A. Steren, X. B. Powers, A. A. Podlesnyak, X.-T. Chen, J. Telser, H. Zhou and Z.-L. Xue, *Polyhedron*, 2020, **184**, 114488.
41. S.-Y. Chen, W. Lv, H.-H. Cui, L. Chen, Y.-Q. Zhang, X.-T. Chen, Z. Wang, Z.-W. Ouyang, H. Yan and Z.-L. Xue, *New J. Chem.*, 2021, **45**, 16852-16861.
42. W. Lv, L. Chen, X.-T. Chen, H. Yan, Z. Wang, Z.-W. Ouyang and Z.-L. Xue, *New J. Chem.*, 2023, **47**, 15553-15560.
43. W. Lv, H.-H. Cui, L. Chen, Y.-Q. Zhang, X.-T. Chen, Z. Wang, Z.-W. Ouyang and Z.-L. Xue, *Dalton Trans.*, 2022, **51**, 7530-7538.
44. H.-H. Cui, M.-M. Ding, X.-D. Zhang, W. Lv, Y.-Q. Zhang, X.-T. Chen, Z. Wang, Z.-W. Ouyang and Z.-L. Xue, *Dalton Trans.*, 2020, **49**, 14837-14846.

45. H.-H. Cui, Y.-Q. Zhang, X.-T. Chen, Z. Wang and Z.-L. Xue, *Dalton Trans.*, 2019, **48**, 10743-10752.
46. S.-Y. Chen, H.-H. Cui, Y.-Q. Zhang, Z. Wang, Z.-W. Ouyang, L. Chen, X.-T. Chen, H. Yan and Z.-L. Xue, *Dalton Trans.*, 2018, **47**, 10162-10171.
47. D. Bloor and G. M. Copland, *Rep. Prog. Phys.*, 1972, **35**, 1173.
48. Y. Rechkemmer, F. D. Breitgoff, M. van der Meer, M. Atanasov, M. Hakl, M. Orlita, P. Neugebauer, F. Neese, B. Sarkar and J. van Slageren, *Nat. Commun.*, 2016, **7**, 10467.
49. R. Marx, F. Moro, M. Dorfel, L. Ungur, M. Waters, S. D. Jiang, M. Orlita, J. Taylor, W. Frey, L. F. Chibotaru and J. van Slageren, *Chem. Sci.*, 2014, **5**, 3287-3293.
50. S. Haas, E. Heintze, S. Zapf, B. Gorshunov, M. Dressel and L. Bogani, *Phys. Rev. B*, 2014, **89**, 174409.
51. P. C. Bunting, M. Atanasov, E. Damgaard-Møller, M. Perfetti, I. Crassee, M. Orlita, J. Overgaard, J. van Slageren, F. Neese and J. R. Long, *Science*, 2018, **362**, eaat7319.
52. M. Gysler, F. El Hallak, L. Ungur, R. Marx, M. Hakl, P. Neugebauer, Y. Rechkemmer, Y. Lan, I. Sheikin, M. Orlita, C. E. Anson, A. K. Powell, R. Sessoli, L. F. Chibotaru and J. van Slageren, *Chem. Sci.*, 2016, **7**, 4347-4354.
53. S. E. Stavretis, D. H. Moseley, F. Fei, H.-H. Cui, Y. Cheng, A. A. Podlesnyak, X. Wang, L. L. Daemen, C. M. Hoffmann, M. Ozerov, Z. Lu, K. Thirunavukkuarasu, D. Smirnov, T. Chang, Y.-S. Chen, A. J. Ramirez-Cuesta, X.-T. Chen and Z.-L. Xue, *Chem. Eur. J.*, 2019, **25**, 15846-15857.
54. A. N. Bone, C. N. Widener, D. H. Moseley, Z. Liu, Z. Lu, Y. Cheng, L. L. Daemen, M. Ozerov, J. Telser, K. Thirunavukkuarasu, D. Smirnov, S. M. Greer, S. Hill, J. Krzystek, K. Holldack, A. Aliabadi, A. Schnegg, K. R. Dunbar and Z.-L. Xue, *Chem. Eur. J.*, 2021, **27**, 11110-11125.
55. P. Tin, S. E. Stavretis, M. Ozerov, J. Krzystek, A. N. Ponomaryov, S. A. Zvyagin, J. Wosnitza, C.-C. Chen, P. P. Y. Chen, J. Telser and Z.-L. Xue, *Appl. Magn. Reson.*, 2020, **51**, 1411-1432.
56. C. N. Widener, A. N. Bone, M. Ozerov, R. Richardson, L. Zheng-Guang, K. Thirunavukkuarasu, D. Smirnov, C. Xue-Tai and X. Zi-Ling, *Chin. J. Inorg. Chem.*, 2020, **36**, 1149.
57. M. Viciano-Chumillas, G. Blondin, M. Clémancey, J. Krzystek, M. Ozerov, D. Armentano, A. Schnegg, T. Lohmiller, J. Telser, F. Lloret and J. Cano, *Chem. Eur. J.*, 2020, **26**, 14242-14251.

58. K. D. Hughey, N. C. Harms, K. R. O'Neal, A. J. Clune, J. C. Monroe, A. L. Blockmon, C. P. Landee, Z. Liu, M. Ozerov and J. L. Musfeldt, *Inorg. Chem.*, 2020, **59**, 2127-2135.
59. J. Vallejo, M. Viciano-Chumillas, F. Lloret, M. Julve, I. Castro, J. Krzystek, M. Ozerov, D. Armentano, G. De Munno and J. Cano, *Inorg. Chem.*, 2019, **58**, 15726-15740.
60. E. Ferentinos, D. Tzeli, S. Sottini, E. J. J. Groenen, M. Ozerov, G. Poneti, K. Kaniewska-Laskowska, J. Krzystek and P. Kyritsis, *Dalton Trans.*, 2023, **52**, 2036-2050.
61. A. Landart-Gereka, M. M. Quesada-Moreno, M. A. Palacios, I. F. Díaz-Ortega, H. Nojiri, M. Ozerov, J. Krzystek and E. Colacio, *Chem. Commun.*, 2023, **59**, 952-955.
62. P. Kumar, D. J. SantaLucia, K. Kaniewska-Laskowska, S. V. Lindeman, A. Ozarowski, J. Krzystek, M. Ozerov, J. Telser, J. F. Berry and A. T. Fiedler, *Inorg. Chem.*, 2020, **59**, 16178-16193.
63. J. G. C. Kragskow, J. Marbey, C. D. Buch, J. Nehrkorn, M. Ozerov, S. Piligkos, S. Hill and N. F. Chilton, *Nat. Commun.*, 2022, **13**, 825.
64. M. Perfetti, M. Gysler, Y. Rechkemmer-Patalen, P. Zhang, H. Taştan, F. Fischer, J. Netz, W. Frey, L. W. Zimmermann, T. Schleid, M. Hakl, M. Orlita, L. Ungur, L. Chibotaru, T. Brock-Nannestad, S. Piligkos and J. van Slageren, *Chem. Sci.*, 2019, **10**, 2101-2110.
65. J. T. Coutinho, M. Perfetti, J. J. Baldoví, M. A. Antunes, P. P. Hallmen, H. Bamberger, I. Crassee, M. Orlita, M. Almeida, J. van Slageren and L. C. J. Pereira, *Chem. Eur. J.*, 2019, **25**, 1758-1766.
66. S. Haas, Ph.D., Universität Stuttgart, 2015.
67. A. Schnegg, J. Behrends, K. Lips, R. Bittl and K. Holldack, *Phys. Chem. Chem. Phys.*, 2009, **11**, 6820-6825.
68. E. Y. Misochko, A. V. Akimov, D. V. Korchagin, J. Nehrkorn, M. Ozerov, A. V. Palii, J. M. Clemente-Juan and S. M. Aldoshin, *Inorg. Chem.*, 2019, **58**, 16434-16444.
69. M. A. Dunstan, R. A. Mole and C. Boskovic, *Eur. J. Inorg. Chem.*, 2019, **2019**, 1090-1105.
70. E. J. L. McInnes, *Struct. Bond. (Single-Molecule Magnets and Related Phenomena)*, 2006, DOI: 10.1007/430_034, 69-102.
71. E. Colacio, J. Ruiz, E. Ruiz, E. Cremades, J. Krzystek, S. Carretta, J. Cano, T. Guidi, W. Wernsdorfer and E. K. Brechin, *Angew. Chem. In. Ed.*, 2013, **52**, 9130-9134.
72. K. S. Pedersen, L. Ungur, M. Sigrist, A. Sundt, M. Schau-Magnussen, V. Vieru, H. Mutka, S. Rols, H. Weihe, O. Waldmann, L. F. Chibotaru, J. Bendix and J. Dreiser, *Chem. Sci.*, 2014, **5**, 1650-1660.

73. X. Feng, J.-L. Liu, K. S. Pedersen, J. Nehrkorn, A. Schnegg, K. Holldack, J. Bendix, M. Sigrist, H. Mutka, D. Samohvalov, D. Aguilà, M.-L. Tong, J. R. Long and R. Clérac, *Chem. Commun.*, 2016, **52**, 12905-12908.
74. M. A. Sørensen, U. B. Hansen, M. Perfetti, K. S. Pedersen, E. Bartolomé, G. G. Simeoni, H. Mutka, S. Rols, M. Jeong, I. Zivkovic, M. Retuerto, A. Arauzo, J. Bartolomé, S. Piligkos, H. Weihe, L. H. Doerrer, J. van Slageren, H. M. Rønnow, K. Lefmann and J. Bendix, *Nat. Commun.*, 2018, **9**, 1292.
75. M. Perfetti, M. A. Sørensen, U. B. Hansen, H. Bamberger, S. Lenz, P. P. Hallmen, T. Fennell, G. G. Simeoni, A. Arauzo, J. Bartolomé, E. Bartolomé, K. Lefmann, H. Weihe, J. van Slageren and J. Bendix, *Adv. Funct. Mater.*, 2018, **28**, 1801846.
76. N. A. Bonde, M. Appel, J. Ollivier, H. Weihe and J. Bendix, *Chem. Commun.*, 2022, **58**, 7431-7434.
77. M. Vonci, M. J. Giansiracusa, W. Van den Heuvel, R. W. Gable, B. Moubaraki, K. S. Murray, D. Yu, R. A. Mole, A. Soncini and C. Boskovic, *Inorg. Chem.*, 2017, **56**, 378-394.
78. M. Vonci, M. J. Giansiracusa, R. W. Gable, W. Van den Heuvel, K. Latham, B. Moubaraki, K. S. Murray, D. Yu, R. A. Mole, A. Soncini and C. Boskovic, *Chem. Commun.*, 2016, **52**, 2091-2094.
79. N. A. Bonde, J. B. Petersen, M. A. Sørensen, U. G. Nielsen, B. Fåk, S. Rols, J. Ollivier, H. Weihe, J. Bendix and M. Perfetti, *Inorg. Chem.*, 2020, **59**, 235-243.
80. M. Perfetti, G. Cucinotta, M.-E. Boulon, F. El Hallak, S. Gao and R. Sessoli, *Chem. Eur. J.*, 2014, **20**, 14051-14056.
81. M. Perfetti, E. Lucaccini, L. Sorace, J. P. Costes and R. Sessoli, *Inorg. Chem.*, 2015, **54**, 3090-3092.
82. L. Rigamonti, N. Bridonneau, G. Poneti, L. Tesi, L. Sorace, D. Pinkowicz, J. Jover, E. Ruiz, R. Sessoli and A. Cornia, *Chem. Eur. J.*, 2018, **24**, 8857-8868.
83. B. Cahier, M. Perfetti, G. Zakhia, D. Naoufal, F. El-Khatib, R. Guillot, E. Rivière, R. Sessoli, A.-L. Barra, N. Guihéry and T. Mallah, *Chem. Eur. J.*, 2017, **23**, 3648-3657.
84. T. Pei, J. O. Thomas, S. Sopp, M.-Y. Tsang, N. Dotti, J. Baugh, N. F. Chilton, S. Cardona-Serra, A. Gaita-Ariño, H. L. Anderson and L. Bogani, *Nat. Commun.*, 2022, **13**, 4506.
85. J. Mayans, L. Tesi, M. Briganti, M.-E. Boulon, M. Font-Bardia, A. Escuer and L. Sorace, *Inorg. Chem.*, 2021, **60**, 8692-8703.
86. F. Pointillart, J. Flores Gonzalez, V. Montigaud, L. Tesi, V. Cherkasov, B. Le Guennic, O. Cador, L. Ouahab, R. Sessoli and V. Kuropatov, *Inorg. Chem. Front.*, 2020, **7**, 2322-2334.

87. M. Perfetti, *Coord. Chem. Rev.*, 2017, **348**, 171-186.
88. K. Bernot, J. Luzon, L. Bogani, M. Etienne, C. Sangregorio, M. Shanmugam, A. Caneschi, R. Sessoli and D. Gatteschi, *J. Am. Chem. Soc.*, 2009, **131**, 5573-5579.
89. G. Cucinotta, M. Perfetti, J. Luzon, M. Etienne, P.-E. Car, A. Caneschi, G. Calvez, K. Bernot and R. Sessoli, *Angew. Chem. In. Ed.*, 2012, **51**, 1606-1610.
90. T. T. da Cunha, J. Jung, M.-E. Boulon, G. Campo, F. Pointillart, C. L. M. Pereira, B. Le Guennic, O. Cador, K. Bernot, F. Pineider, S. Golhen and L. Ouahab, *J. Am. Chem. Soc.*, 2013, **135**, 16332-16335.
91. Y. Fang, M.-X. Xu, Y.-C. Hui, H.-L. Sun, X. Yan and S.-D. Jiang, *J. Magn. Magn. Mater.*, 2019, **490**, 165475.
92. W. Wernsdorfer, *Adv. Chem. Phys.*, 2001, **118**, 99-190.
93. G. Novitchi, S. Jiang, S. Shova, F. Rida, I. Hlavička, M. Orlita, W. Wernsdorfer, R. Hamze, C. Martins, N. Suaud, N. Guihéry, A.-L. Barra and C. Train, *Inorg. Chem.*, 2017, **56**, 14809-14822.
94. J. Liu, Y.-C. Chen, J.-L. Liu, V. Vieru, L. Ungur, J.-H. Jia, L. F. Chibotaru, Y. Lan, W. Wernsdorfer, S. Gao, X.-M. Chen and M.-L. Tong, *J. Am. Chem. Soc.*, 2016, **138**, 5441-5450.
95. L. Chen, J. Wang, J.-M. Wei, W. Wernsdorfer, X.-T. Chen, Y.-Q. Zhang, Y. Song and Z.-L. Xue, *J. Am. Chem. Soc.*, 2014, **136**, 12213-12216.
96. N. J. Wolford, A. Radovic and M. L. Neidig, *Dalton Trans.*, 2021, **50**, 416-428.
97. S. Piligkos, L. D. Slep, T. Weyhermüller, P. Chaudhuri, E. Bill and F. Neese, *Coord. Chem. Rev.*, 2009, **253**, 2352-2362.
98. J. van Slageren, S. Piligkos and F. Neese, *Dalton Trans.*, 2010, **39**, 4999-5004.
99. V. N. Nemykin, B. R. Schrage, D. E. Nevonen, L. A. Harrison, K. M. E. Newman, V. K. Paidi and J. v. Lierop, *Inorg. Chem.*, 2023, **62**, 10203-10220.
100. R. Marin, G. Brunet and M. Murugesu, *Angew. Chem. In. Ed.*, 2021, **60**, 1728-1746.
101. J.-T. Chen, T.-D. Zhou and W.-B. Sun, *Dalton Trans.*, 2023, **52**, 4643-4657.
102. M. Perfetti, F. Pointillart, O. Cador, L. Sorace and L. Ouahab, in *Molecular Magnetic Materials*, 2017, DOI: https://doi.org/10.1002/9783527694228.ch14, pp. 345-368.
103. Z. Zhu, X.-L. Li, S. Liu and J. Tang, *Inorg. Chem. Front.*, 2020, **7**, 3315-3326.
104. J.-H. Jia, Q.-W. Li, Y.-C. Chen, J.-L. Liu and M.-L. Tong, *Coord. Chem. Rev.*, 2019, **378**, 365-381.
105. M. T. Dove, *Introduction to Lattice Dynamics*, Cambridge University Press, 1993.

106. P. C. H. Mitchell, S. F. Parker, A. J. Ramirez-Cuesta and J. Tomkinson, *Vibrational Spectroscopy with Neutrons: With Applications in Chemistry, Biology, Materials Science and Catalysis*, World Scientific Publishing Company, 2005.
107. A. Lunghi, in *Computational Modelling of Molecular Nanomagnets*, ed. G. Rajaraman, Springer International Publishing, Cham, 2023, pp. 219-289.
108. A. Lunghi and S. Sanvito, *Science Advances*, 2019, **5**, eaax7163.
109. A. Lunghi and S. Sanvito, *J. Chem. Phys.*, 2020, **153**, 174113.
110. A. Lunghi, *Sci. Adv.*, 2022, **8**, eabn7880.
111. A. Lunghi, F. Totti, S. Sanvito and R. Sessoli, *Chem. Sci.*, 2017, **8**, 6051-6059.
112. C. A. P. Goodwin, F. Ortu, D. Reta, N. F. Chilton and D. P. Mills, *Nature*, 2017, **548**, 439-442.
113. M. A. Dunstan, M. J. Giansiracusa, M. Vonci, S. Calvello, D. Yu, A. Soncini, C. Boskovic and R. A. Mole, *Chem. Sci.*, 2023, **14**, 3990-4001.
114. L. Escalera-Moreno, N. Suaud, A. Gaita-Ariño and E. Coronado, *J. Phys. Chem. Lett.*, 2017, **8**, 1695-1700.
115. A. Lunghi, F. Totti, R. Sessoli and S. Sanvito, *Nat. Commun.*, 2017, **8**, 14620.
116. A. L. Blockmon, A. Ullah, K. D. Hughey, Y. Duan, K. R. O'Neal, M. Ozerov, J. J. Baldoví, J. Aragó, A. Gaita-Ariño, E. Coronado and J. L. Musfeldt, *Inorg. Chem.*, 2021, **60**, 14096-14104.
117. R. Mirzoyan, N. P. Kazmierczak and R. G. Hadt, *Chem. Eur. J.*, 2021, **27**, 9482-9494.
118. K. Chakarawet, M. Atanasov, J. E. Ellis, W. W. Lukens, Jr., V. G. Young, Jr., R. Chatterjee, F. Neese and J. R. Long, *Inorg. Chem.*, 2021, **60**, 18553-18560.
119. N. J. Higdon, A. T. Barth, P. T. Kozlowski and R. G. Hadt, *J. Chem. Phys.*, 2020, **152**, 204306.
120. L. Gu and R. Wu, *Phys. Rev. Lett.*, 2020, **125**, 117203.
121. K. Irländer and J. Schnack, *Phys. Rev. B*, 2020, **102**, 054407.
122. L. Escalera-Moreno, J. J. Baldoví, A. Gaita-Ariño and E. Coronado, *Chem. Sci.*, 2020, **11**, 1593-1598.
123. L. Bogani, L. Cavigli, M. Gurioli, R. L. Novak, M. Mannini, A. Caneschi, F. Pineider, R. Sessoli, M. Clemente-León, E. Coronado, A. Cornia and D. Gatteschi, *Adv. Mater.*, 2007, **19**, 3906-3911.
124. S. E. Stavretis, E. Mamontov, D. H. Moseley, Y. Cheng, L. L. Daemen, A. J. Ramirez-Cuesta and Z.-L. Xue, *Phys. Chem. Chem. Phys.*, 2018, **20**, 21119-21126.

125. S. E. Stavretis, M. Atanasov, A. A. Podlesnyak, S. C. Hunter, F. Neese and Z.-L. Xue, *Inorg. Chem.*, 2015, **54**, 9790.
126. L. Chen, H.-H. Cui, S. E. Stavretis, S. C. Hunter, Y.-Q. Zhang, X.-T. Chen, Y.-C. Sun, Z. Wang, Y. Song, A. A. Podlesnyak, Z.-W. Ouyang and Z.-L. Xue, *Inorg. Chem.*, 2016, **55**, 12603-12617.
127. S. C. Hunter, A. A. Podlesnyak and Z.-L. Xue, *Inorg. Chem.*, 2014, **53**, 1955-1961.
128. Infrared/Terahertz Magneto Optics in DC Fields, website: https://nationalmaglab.org/user-facilities/dc-field/measurement-techniques/magneto-optics-ir-thz-dc/ (accessed on October 22, 2023).
129. Raman Magneto-Spectroscopy in DC Fields, website: https://nationalmaglab.org/user-facilities/dc-field/measurement-techniques/raman-dc/ (accessed on October 22, 2023).
130. CNCS, website: https://neutrons.ornl.gov/cncs (accessed on October 22, 2023).
131. VISION, website: https://neutrons.ornl.gov/vision (accessed on October 22, 2023).
132. DCS, website: https://ncnr.nist.gov/instruments/dcs/ (accessed on October 22, 2023).
133. G. C. Brackett, P. L. Richards and W. S. Caughey, *J. Chem. Phys.*, 1971, **54**, 4383-4401.
134. G. C. Brackett, Ph.D. dissertation, University of California, Berkeley, 1970.
135. P. L. Richards, W. S. Caughey, H. Eberspaecher, G. Feher and M. Malley, *J. Chem. Phys.*, 1967, **47**, 1187-1188.
136. F. A. Cotton, *Chemical Applications of Group Theory, 3rd Ed., Chapters 9 and 10*, Wiley, New York, 3 edn., 1990.
137. R. J. H. Clark and T. J. Dines, *Advances in Infrared and Raman Spectroscopy*, 1982, **9**, 282-360.
138. D. A. Long, *The Raman Effect. A Unified Treatment of the Theory of Raman Scattering by Molecules. Ch. 9, "Normal and Resonance Electronic and Vibronic Raman Scattering," pp. 289-302*, Wiley, West Sussex, UK, 2002.
139. .
140. V. P. Gnezdilov, V. V. Eremenko, A. V. Peschansky and V. I. Fomin, *Fiz. Nizk. Temp. (Low. Temp. Phys.)*, 1991, **17**, 253-258.
141. P. M. Champion and A. J. Sievers, *J. Chem. Phys.*, 1977, **66**, 1819-1825.
142. J. Krzystek, D. Smirnov, C. Schlegel, J. v. Slageren, J. Telser and A. Ozarowski, *J. Magn. Reson.*, 2011, **213**, 158-165.
143. Z.-L. Xue, A. J. Ramirez-Cuesta, C. M. Brown, S. Calder, H. Cao, B. C. Chakoumakos, L. L. Daemen, A. Huq, A. I. Kolesnikov, E. Mamontov, A. A. Podlesnyak and X. Wang, *Eur. J. Inorg. Chem.*, 2019, **2019**, 1065-1089.

144. M. L. Baker, T. Guidi, S. Carretta, J. Ollivier, H. Mutka, H. U. Güdel, G. A. Timco, E. J. L. McInnes, G. Amoretti, R. E. P. Winpenny and P. Santini, *Nat. Phys.*, 2012, **8**, 906-911.
145. E. Garlatti, T. Guidi, S. Ansbro, P. Santini, G. Amoretti, J. Ollivier, H. Mutka, G. Timco, I. J. Vitorica-Yrezabal, G. F. S. Whitehead, R. E. P. Winpenny and S. Carretta, *Nat. Commun.*, 2017, **8**, 14543.
146. A. Furrer, J. Mesot and T. Strässle, *Neutron Scattering in Condensed Matter Physics*, World Scientific, 2009.
147. J. R. D. Copley and J. C. Cook, *Chem. Phys.*, 2003, **292**, 477-485.
148. G. E. Bacon, *Neutron Scattering in Chemistry*, Butterworth, London, 1977.
149. G. L. Squires, *Introduction to the Theory of Thermal Neutron Scattering*, Cambridge University Press, 1978.
150. P. Tin, M. J. Jenkins, J. Xing, N. Caci, Z. Gai, R. Jin, S. Wessel, J. Krzystek, C. Li, L. L. Daemen, Y. Cheng and Z.-L. Xue, *Nat. Commun.*, 2023, **14**, 5454.
151. P. A. Seeger, L. L. Daemen and J. Z. Larese, *Nucl. Instr. Meth. Phys. Res. A*, 2009, **604**, 719-728.
152. S. F. Parker, A. J. Ramirez-Cuesta and L. Daemen, *Spectrochim. Acta A*, 2018, **190**, 518-523.
153. D. Gatteschi, *J. Phys. Chem. B*, 2000, **104**, 9780-9787.
154. M. Sigrist, P. L. W. Tregenna-Piggott, K. S. Pedersen, M. A. Sørensen, A.-L. Barra, J. Hauser, S.-X. Liu, S. Decurtins, H. Mutka and J. Bendix, *Eur. J. Inorg. Chem.*, 2015, **2015**, 2683-2689.
155. K. S. Pedersen, M. Sigrist, H. Weihe, A. D. Bond, C. A. Thuesen, K. P. Simonsen, T. Birk, H. Mutka, A.-L. Barra and J. Bendix, *Inorg. Chem.*, 2014, **53**, 5013-5019.
156. S. K. Singh, K. S. Pedersen, M. Sigrist, C. A. Thuesen, M. Schau-Magnussen, H. Mutka, S. Piligkos, H. Weihe, G. Rajaraman and J. Bendix, *Chem. Commun.*, 2013, **49**, 5583-5585.
157. J. Dreiser, K. S. Pedersen, A. Schnegg, K. Holldack, J. Nehrkorn, M. Sigrist, P. Tregenna-Piggott, H. Mutka, H. Weihe, V. S. Mironov, J. Bendix and O. Waldmann, *Chem. Eur. J.*, 2013, **19**, 3693-3701.
158. J. Dreiser, A. Schnegg, K. Holldack, K. S. Pedersen, M. Schau-Magnussen, J. Nehrkorn, P. Tregenna-Piggott, H. Mutka, H. Weihe, J. Bendix and O. Waldmann, *Chem. Eur. J.*, 2011, **17**, 7492-7498.
159. S. I. Klokishner, S. M. Ostrovsky, O. S. Reu, A. V. Palii, P. L. W. Tregenna-Piggott, T. Brock-Nannestad, J. Bendix and H. Mutka, *J. Phys. Chem. C*, 2009, **113**, 8573-8582.

160. P. L. W. Tregenna-Piggott, D. Sheptyakov, L. Keller, S. I. Klokishner, S. M. Ostrovsky, A. V. Palii, O. S. Reu, J. Bendix, T. Brock-Nannestad, K. Pedersen, H. Weihe and H. Mutka, *Inorg. Chem.*, 2009, **48**, 128-137.
161. M. Hennion, L. Pardi, I. Mirebeau, E. Suard, R. Sessoli and A. Caneschi, *Phys. Rev. B*, 1997, **56**, 8819-8827.
162. R. Basler, C. Boskovic, G. Chaboussant, H. U. Güdel, M. Murrie, S. T. Ochsenbein and A. Sieber, *ChemPhysChem*, 2003, **4**, 910-926.
163. D. Gatteschi, *J. Phys. Chem. B*, 2000, **104**, 9780-9787.
164. M. A. Dunstan, R. A. Mole and C. Boskovic, *Eur. J. Inorg. Chem.*, 2019, **2019**, 1090.
165. S. Gómez-Coca, A. Urtizberea, E. Cremades, P. J. Alonso, A. Camón, E. Ruiz and F. Luis, *Nat. Commun.*, 2014, **5**, 4300.
166. P. Zhang, L. Zhang, C. Wang, S. Xue, S.-Y. Lin and J. Tang, *J. Am. Chem. Soc.*, 2014, **136**, 4484-4487.
167. A. Landart-Gereka, M. M. Quesada-Moreno, I. F. Díaz-Ortega, H. Nojiri, M. Ozerov, J. Krzystek, M. A. Palacios and E. Colacio, *Inorg. Chem. Front.*, 2022, **9**, 2810-2831.
168. K. S. Pedersen, D. N. Woodruff, S. K. Singh, A. Tressaud, E. Durand, M. Atanasov, P. Perlepe, K. Ollefs, F. Wilhelm, C. Mathonière, F. Neese, A. Rogalev, J. Bendix and R. Clérac, *Chem. Eur. J.*, 2017, **23**, 11244-11248.
169. G. Kresse and J. Furthmüller, *Phys. Rev. B*, 1996, **54**, 11169-11186.
170. M. L. Baker, S. J. Blundell, N. Domingo and S. Hill, *Struct. Bond.*, 2015, **164**, 231-291.
171. S. K. Singh, J. Eng, M. Atanasov and F. Neese, *Coord. Chem. Rev.*, 2017, **344**, 2-25.
172. P. E. Blöchl, *Phys. Rev. B*, 1994, **50**, 17953-17979.
173. G. Kresse and D. Joubert, *Phys. Rev. B*, 1999, **59**, 1758-1775.
174. C. Cohen-Tannoudji, F. Laloe and B. Diu, *Quantum Mechanics*, Wiley, New York, 1977.
175. M. M. Roessler and E. Salvadori, *Chem. Soc. Rev.*, 2018, **47**, 2534-2553.
176. A. C. Rizzi, N. I. Neuman, P. J. González and C. D. Brondino, *Eur. J. Inorg. Chem.*, 2016, **2016**.
177. N. F. Chilton, R. P. Anderson, L. D. Turner, A. Soncini and K. S. Murray, *J. Comput. Chem.*, 2013, **34**, 1164-1175.

Table of Contents entry

Magnetic anisotropy and spin-phonon coupling are key properties of single-molecule magnets. The use of far-IR (FIRMS), Raman magneto-spectroscopy (RaMS), and inelastic neutron scattering (INS) to determine the magnetic properties is highlighted.

The original with high resolution of the following graphic is in a pptx file submitted with the manuscript.